Epitaxial growth and band bending of *n*- and *p*-type Ge on GaAs(001)

S. A. Chambers and T. J. Irwin
Materials and Devices Laboratory, Boeing Electronics, High Technology Center, P.O. Box 24969, Seattle, Washington 98124-6269
(Received 12 May 1988)

We have combined high-resolution x-ray photoelectron spectroscopy, low-energy electron diffraction, and x-ray photoelectron diffraction to examine the interface structure and band-bending characteristics of *n*- and *p*-type Ge epilayers grown on semi-insulating GaAs(001). The first monolayer of Ge intermixes with atoms in the near-surface region to yield a complex structure. Subsequent Ge monolayers grow epitaxially but exhibit surface roughness in the form of local variation in layer thickness of the order of 2–3 monolayers (3–4 Å), in agreement with previous reflection high-energy electron diffraction measurements obtained during continuous overlayer growth. The growth of undoped (which is actually *p* type) and As-doped Ge overlayers results in Schottky-barrier-height changes of $+0.05$ and -0.35 eV, respectively, relative to the clean-surface value of 0.83 ± 0.05 eV. Furthermore, the barrier height correlates directly with dopant level in the Ge epilayer. In contrast, the valence band offset is independent of dopant level in the Ge film and maintains a constant value of 0.60 ± 0.05 eV. With the exception of the barrier height of the starting surface, these results are the same as those obtained on *n*-type substrates, further supporting the conclusion that barrier-height formation and band-offset development occur independently.

I. INTRODUCTION

The Ge/GaAs(001) heterojunction interface has been the subject of intense research over the past several years. The excellent 99.87% lattice match between Ge and GaAs makes possible high-quality epitaxial growth with relative ease. Investigators have examined surface- and thin-film structure,[1–5] electrical characteristics,[6–9] and superlattice properties for this system.[2,4,10] The vast majority of previous work has been done in one of two ways. Either a buffer layer of GaAs was deposited on (001)-oriented substrates, or chemically cleaned substrates were Ar-ion sputtered and annealed in either ultrahigh vacuum (UHV) or a high partial pressure of arsenic before growing Ge overlayers or Ge/GaAs superlattices. These preparation techniques leave the surface in one of several reconstructions—either Ga-rich (4×2), $c(8\times2)$, and (4×6), or As-rich (1×2), (2×4), $c(2\times8)$, and $c(4\times4)$. Past structural studies have centered around reflection high-energy electron diffraction (RHEED) measurements during growth[1–3] and transmission electron microscopy (TEM) of completed superlattices.[2,4] RHEED patterns suggest that Ge growth on GaAs results in reasonably smooth surfaces whereas subsequent growth of GaAs on Ge leads to rougher surfaces on an atomic scale for samples grown in the (001) orientation.[1–2] TEM investigations show that the structural quality of completed superlattices is quite good, although antiphase domain boundaries do occur in GaAs layers grown on (001)-oriented structures.[2,4] In all cases where electron diffraction data were reported, the Ge overlayer was observed to exhibit a (2×2) surface periodicity.[1–3]

Electronically, it has been shown that the Fermi-level position within the band gap of *n*-type GaAs can be moved to higher energy by doping the Ge epilayer with arsenic or phosphorus,[11] and that such Fermi-level movement is independent of the valence-band discontinuity.[12] The latter result challenges the applicability of a defect model to barrier-height formation in heterojunctions. Therefore, the Ge/GaAs interface is a good candidate for fundamental studies in that it grows with a predictable structure, exhibits interesting electrical properties, and may serve as a good test case for increasingly refined theories of heterostructure interface formation. However, there are several unanswered questions related to both the structure and electronic behavior. Specifically, the structural nature of the interface and the exact mode of growth of the first few epitaxial layers are not known. Also, it has not yet been established how band-bending behavior at the interface depends on doping in the GaAs substrate, and how thermally stable the doped Ge overlayer is; arsenic tends to be rather mobile and volatile in a wide variety of systems.

In the present work we report results for doped and undoped Ge epilayer growth on GaAs(001) surfaces that were neither sputtered and annealed in vacuum nor treated with a thick buffer layer of GaAs prior to overlayer growth. Rather, we have used native GaAs(001) surfaces that were very carefully cleaned by chemical means and lightly oxidized prior to insertion in a molecular-beam-epitaxy (MBE) chamber. Oxide removal was accomplished under vacuum by briefly flashing to the minimum necessary temperature, and no GaAs buffer layer was grown. The resulting surfaces and interfaces were then studied *in situ* using a combination of techniques, including a relatively new structural technique (x-ray photoelectron Auger electron diffraction) which yields unique information about the structure and morphology of ultrathin epitaxial layers. We have combined high-resolution x-ray photoelectron spectroscopy (XPS), low-

energy electron diffraction (LEED), and x-ray photoelectron diffraction (XPD) to investigate the structural behavior of the Ge/GaAs(001) interface when grown in a layer-by-layer fashion. Furthermore, we have extended previous work on the band-bending caused by As doping of the Ge epilayer on n-type GaAs to include semi-insulating GaAs substrates. Finally, we have examined the dependence of the Schottky-barrier height (SBH) on dopant level in the Ge and the thermal stability of the system. The remainder of this paper is partitioned as follows. Section II describes the experimental details, Sec. III contains the results and discussion, and Sec. IV gives our conclusions.

II. EXPERIMENTAL DETAILS

Our experimental apparatus consists of a simple two-source MBE chamber appended to an analytical chamber equipped with probes chosen to yield structural, chemical, and electronic data for surfaces and interfaces. The system includes a Surface Science Instruments Series 300 XPS spectrometer which has been modified for scanned-angle XPD measurements, a sample manipulator with two-axis rotational and xyz translational degrees of freedom, a Leybold-Heraeus Ar-ion sputter gun, and a Princeton Research Instruments reverse-view LEED system. The XPS spectrometer is equipped with a monochromatic, focused Al $K\alpha$ x-ray source, a hemispherical analyzer, a multichannel detector, and an externally-actuated aperture system enabling XPD measurements with one of three angular resolutions. All XPD results described in the present work employed a full angle of acceptance of 5° in both polar and azimuthal directions, and an x-ray beam diameter of 1000 μm. The base pressure of both chambers is 6×10^{-11} torr.

Semi-insulating (Cr-doped, 1×10^{7} Ω cm) GaAs samples oriented to within 0.5° of (001) were prepared by two different chemical cleanings. Following a standard degrease in 1,1,1-trichloroethane, acetone, and methanol, the wafers were etched in either $5H_2SO_4/1H_2O_2/1H_2O$ for 30 sec or $1NH_4OH/1H_2O_2/3H_2O$ for 3 min, dipped in ultrapure deionized water (6–7 parts per billion total organic content), and rinsed for 5 min in flowing ultrapure deionized water. Samples were then air dried in a class-100 clean room, mounted on a Mo sample stub with a thin, screw-held Ta shim, and heated in clean room air for 2–3 min at 190 °C to form a volatile oxide and volatile carbonaceous species.[13] The sample assembly was then quickly transferred to the spectrometer loadlock, roughed down to the low 10^{-7}-torr range with a turbomolecular pump, and transferred into the MBE chamber. Following heating in UHV for 1.5 h at 270 °C, the sample was heated momentarily to 550 °C. The time required to raise the temperature of the sample block from 270 to 550 °C was approximately 3–4 min, and the sample heater was turned off immediately upon reaching 550 °C. The resulting surface was free of impurities, as judged by XPS, and exhibited a $c(2\times2)$ LEED pattern.

MBE growth was carried out with the substrate held at 320 °C. 99.999%-pure Ge was evaporated from a tungsten coil at rates varying from 1 to 20 monolayers per minute, depending on the experiment. Ge flux was monitored by means of a quartz-crystal oscillator. As_2 was liberated by resistively heating a chunk of polycrystalline GaAs held in a tungsten boat until a small but nonzero arsenic flux was detected on a quartz-crystal oscillator and a pressure rise was detected in the chamber. Ge and As_2 were then coevaporated. After overlayer growth, the sample was cooled to room temperature, transferred to the analytical chamber and picked up by the two-axis manipulator, which in turn accesses any of the experimental probes and permits XPD measurements with 270° of azimuthal and 180° of polar angle motion.

Angular calibration and orientation of the sample were accomplished as follows. A small He-Ne laser in a vertical orientation was mounted outside the chamber so that the laser beam could be directed through a viewpoint onto the GaAs surface and reflected backward, thereby allowing approximate calibration of the polar angle (θ). The LEED pattern was then used to find the approximate location of the (010) azimuthal plane. An azimuthal scan of the Ga and As $3d$ intensity was then performed at $\theta=45°$ to locate (010) to within the angular precision of the manipulator, which is $\pm0.5°$. Major diffraction peaks occur for high-energy Auger and photoelectron emission along low-index directions and these features are very useful for angular alignment.[14] Calibration of the polar angle was done the same way; scanning through normal emission in the (010) azimuthal plane shows pronounced maxima in both Ga and As $3d$ intensity at $\theta=90°$ as a result of forward scattering along [001]. Two iterations of this procedure were typically required to fully align the surface to the spectrometer in both polar and azimuthal directions.

III. RESULTS AND DISCUSSION

A. Structure and morphology of the overlayer

The atom-specific nature of photoelectron and Auger-electron diffraction affords some unique advantages for studying epitaxial thin-film growth. For overlayers containing different atoms than those found in the substrate, one can measure the angular distributions of photoelectron intensity for those atoms found only in the overlayer and thereby completely eliminate contributions from the substrate. As has been shown previously, these closely related techniques yield detailed information about interface structure and thin-film morphology.[15,16] Interpretation of the data is readily accomplished through the use of a kinematical or single-scattering cluster formalism in which trial geometries are used to generate theoretical angular distributions for comparison with experiment. We have followed this approach in characterizing the structure of the Ge/GaAs(001) interface when grown in a layer-by-layer fashion. Details of the calculations are described elsewhere.[16,17]

In Fig. 1 we show a unit cell of zinc-blende GaAs and superimpose upon it the convention we have used in aligning high-symmetry planes in the material with our experimental geometry. In addition, a schematic representation of the geometry of our XPD system is shown in

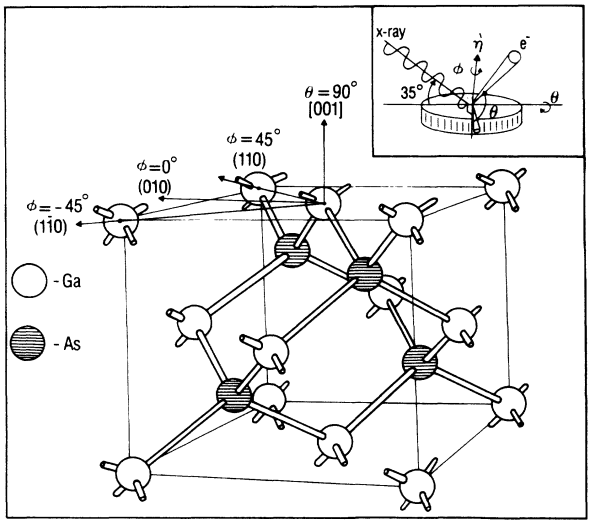

FIG. 1. The structure of zinc-blende GaAs(001) showing the relationship between low-index directions in the material and the angular coordinates of the spectrometer.

the inset. We have measured Ga, As, and Ge $3d$ photoelectron angular distributions as a function of polar angle (θ) in three different azimuthal planes: (010) for which we define the azimuthal angle (ϕ) as zero, (1$\bar{1}$0) for which $\phi=-45°$, and (110) at $\phi=+45°$. Normal emission along [001] is defined as $\theta=90°$.

In Fig. 2 we show measured and calculated Ga and As $3d$ polar-angle distributions (PAD's) in the three aforementioned azimuthal planes for the clean GaAs substrate. We have assumed in the calculations that the surface possesses a Ga-terminated, bulklike (i.e., unreconstructed) geometry and have used a cluster size of 12 atomic layers with 169 atoms per layer. Comparison of experimental and theoretical PAD's allows the (110) azimuthal plane to be distinguished from the (1$\bar{1}$0) plane. As shown in Fig. 2, there is no difference between the Ga $3d$ and As $3d$ PAD's in (010); both show zeroth-order forward-scattering-induced peaks along [101] ($\theta=45°$) and along [001] ($\theta=90°$), and peaks resulting from more complex interference phenomena between 60 and 80°.[18] This result is a natural consequence of the symmetry of the crystal structure; the (010) azimuth consists of identical sublattices of Ga and As atoms displaced by $(\frac{1}{4},\frac{1}{4},\frac{1}{4})$. Moreover, agreement with theory is quite good, the only significant problem being the discrepancy between the measured and calculated intensity of the peak at 45°. However, there are major differences between the Ga and As $3d$ PAD's in both (110) and (1$\bar{1}$0). Most notable is the fact that the Ga $3d$ PAD in (1$\bar{1}$0) closely resembles the As $3d$ PAD in (110) while the As $3d$ PAD in (1$\bar{1}$0) is very similar to the Ga $3d$ PAD in (110). This result is also a natural consequence of the symmetry of the crystal, as can be appreciated by examination of Fig. 1. As atoms experience nearest-neighbor forward scatterers in the Ga atoms at $\theta=35°$ in (110) whereas Ga atoms experience the same in As atoms at $\theta=35°$ in (1$\bar{1}$0). These observations and conclusions are consistent with previous

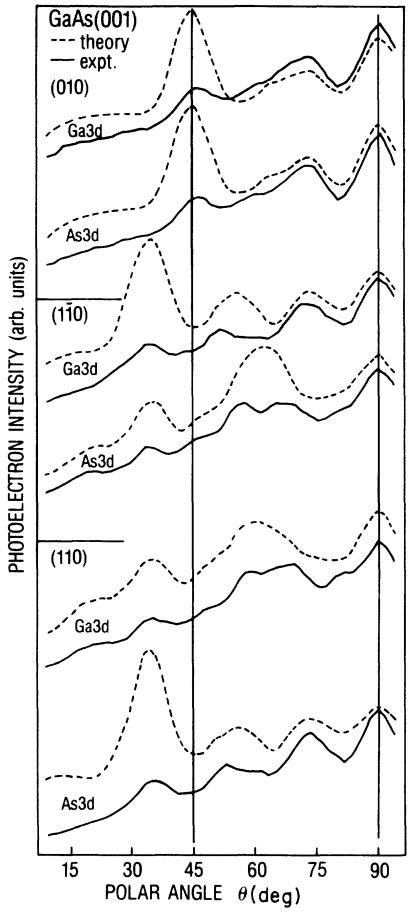

FIG. 2. Experimental and theoretical polar-angle distributions (PAD's) of Ga and As $3d$ intensity for clean GaAs(001) in the (010), (1$\bar{1}$0), and (110) azimuths.

XPD work on GaAs(001) surfaces,[19–21] and allow us to unambiguously characterize the crystallographic orientation of the substrate.

Agreement with theory is also quite good in the (1$\bar{1}$0) and (110) azimuths. All major features seen in the measured PAD's are reproduced in the calculated PAD's. However, there continues to be a large difference between the measured and calculated intensity of the forward-scattering-induced peak at 35° in both azimuths, similar to what was observed at 45° in (010). The most probable cause of this result is the neglect of multiple-scattering[22] and spherical-wave effects,[23] which is known to cause calculated diffraction features along low-index directions to be more intense than the associated experimental values. There is also an observed splitting in the peak at 60° for Ga $3d$ emission in (110) and As $3d$ emission in (1$\bar{1}$0) which is not predicted by theory. However, overall agreement between theory and experiment is in general quite good for all three azimuths, and establishes that this approach will be effective in tracking the structure of the Ge overlayers. In addition, the high level of agreement between theory and experiment demonstrates that polar XPD scans are not particularly sensitive to the surface reconstruction, a consequence of the ~25 Å electron

escape depth for Ga and As 3d photoelectrons excited with Al $K\alpha$ x radiation. Indeed, PAD's we have obtained on the $c(8\times2)$ reconstruction (not shown) are virtually the same as those shown in Fig. 2, in which the surface exhibited a $c(2\times2)$ LEED pattern.

In Fig. 3 we show a conventional growth-attenuation plot for Ge 3d and Ga 3d intensity as a function of Ge coverage in both monolayers (ML) and angstroms. All data points were obtained at $\theta=35°$ in the (010) azimuth which, as Figs. 2 and 4 show, is conveniently away from any diffraction features. In order to illustrate the behavior of the Ga 3d reduced intensity we anticipate if perfect layer-by-layer growth occurs, we have also plotted as a dashed line the expected rate of decay of the Ga 3d reduced intensity using an inelastic mean free path of 25 Å, which is approximately correct for photoelectrons of $\sim$1450 eV kinetic energy.[24] The drop in Ga 3d intensity between 0 and 1 ML is significantly steeper than what is observed between 1 and 2 ML, for which there is no measurable decrease. On the other hand, the Ge 3d intensity increases steadily over this coverage range. The rate of increase of Ge 3d intensity and the rate of decrease in Ga 3d intensity are quite uniform for coverages above 2 ML, and the overall level of agreement between the measured and calculated attenuation curves is good. In fact, the slope of the Ga 3d reduced-intensity plot over the coverage range from 2 to 7 ML yields a mean free path of 27.3 Å, in excellent agreement with a previously reported value of 26.6 Å for 1450-eV photoelectron emission in Ge.[25] Moreover, the LEED pattern changes from $c(2\times2)$ characteristic of the GaAs substrate to a weak $p(2\times1)$ at a coverage of 1 ML. From 2 to 5 ML, the $p(2\times1)$ patterns sharpens considerably and then converts to a $p(2\times2)$ pattern at 6 ML, which persists for all higher coverages examined (up to 100 ML). Taken together, the LEED and attenuation-growth data suggest that the mode of growth is nominally layer by layer and essentially uniform, as opposed to island formation. Phase-segregated island growth would be manifest by a considerably slower rate of attenuation for the substrate photoelectron intensity, and by persistence of the substrate LEED pattern after Ge deposition, provided island growth left patches of exposed substrate with dimensions of the order of the coherence length of the LEED beam. In addition, the Ga 3d attenuation behavior establishes an independent calibration for our Ge-coverage scale.

To probe the structure of the evolving overlayer in more detail, we now turn to XPD results. In Figs. 4–6 we show Ge 3d intensity-derived PAD's in the (010), (110), and (1$\bar{1}$0) azimuthal planes. In the left-hand panels, we present theoretical results in which perfect layer-by-layer epitaxial growth is assumed. The corresponding experimental data are shown in the right-hand panels. Turning first to the calculated PAD's, the curves for 1 ML coverage are essentially featureless in all three azimuths. The absence of peaks is simply the result of an absence of atoms on top of the first ML of Ge to act as forward scatterers for photoelectrons emitted from first-layer Ge atoms. At 2 ML, a large peak develops at $\theta=35°$, but only in (110); no features appear in (1$\bar{1}$0) or (010). The origin of the peak at 35° in (110) is the presence of second-layer Ge atoms at these angular coordinates which can act as forward scatterers for photoelectrons generated in the first layer. (This result can be visualized by referring to Fig. 1 and projecting the positions of atoms in the first two epitaxial layers of Ge.) At 3 ML, peaks appear at 45° in (010) and at 35° in (1$\bar{1}$0) as atoms in this layer directly forward-scatter photoelectrons generated in the underlayers. At 5 ML, we see the appearance of a peak at 90° in all three azimuths as a sufficient number of layers is present to provide scattering sites along the surface normal. These calculations demonstrate that the high degree of forward scattering at the kinetic energy of Ge 3d photoemission (1457 eV) provides a

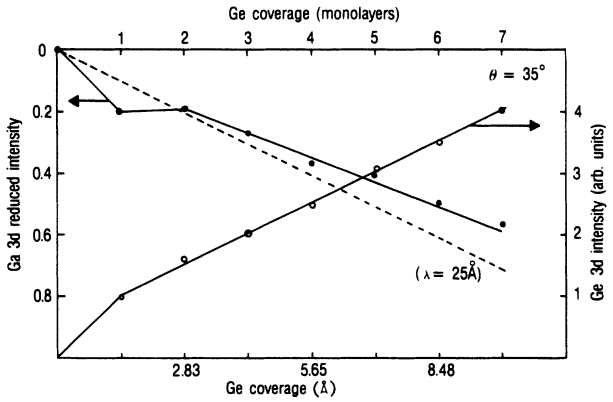

FIG. 3. Growth and attenuation curves for epitaxial Ge grown on GaAs(001) at 320 °C. The Ga 3d intensity is expressed as a reduced intensity, defined as $\ln[I(d_{Ge})/I(0)]$ where d_{Ge} is the Ge overlayer thickness is angstroms. The dashed line is the Ga 3d signal attenuation expected if the overlayer grows in a perfect layer-by-layer fashion, assuming an escape depth of 25 Å for Ga 3d photoemission.

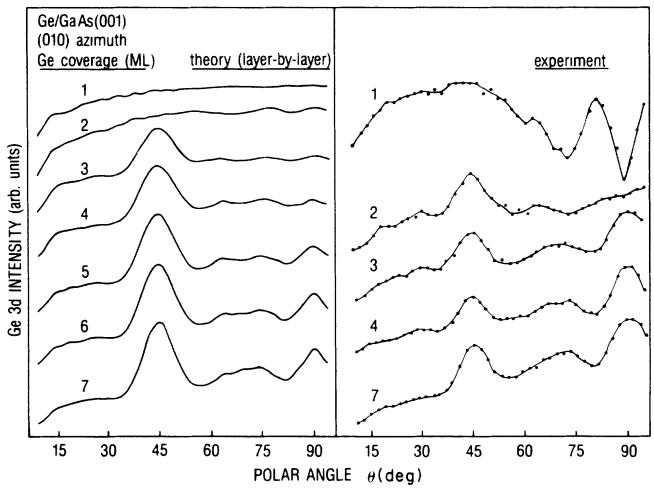

FIG. 4. Experimental and theoretical Ge 3d polar-angle distributions (PAD's) in the (010) azimuth as a function of coverage for Ge growth on GaAs(001) at 320 °C. The theoretical calculations assume no intermixing at the interface and perfect epitaxial growth.

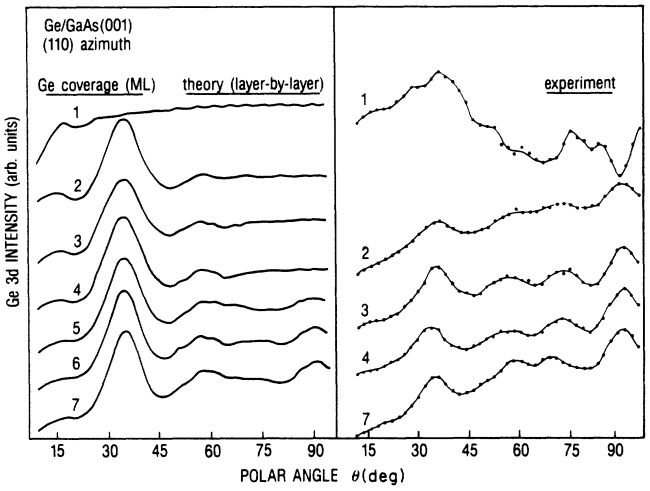

FIG. 5. Same as Fig. 4, only in the (110) azimuth.

direct and sensitive probe of the layer structure in the early stages of epitaxy, as has been noted in earlier work.[18,26–28]

Turning our attention to the experimental data, we see something quite different from the theoretical expectations, particularly at 1 ML. Rather than being featureless, the 1-ML PAD's in all three azimuths show considerable structure, particularly at higher polar angles. Qualitatively, this result strongly suggests intermixing of the first monolayer with the substrate. Previous investigations of the $CoSi_2$/Si(111),[29] Cu/Si(111),[17] NiO/Ni(001),[30] and O/Cu(001) (Ref. 31) systems demonstrate that high-energy Auger-electron–x-ray-photoelectron diffraction can be used to determine whether adatoms reside above or below the surface layer of the substrate, and the quantitative structural details of the interface. When adatoms assume positions *below* the surface [as in the case of $CoSi_2$ on Si(111) and NiO on Ni(001)], they are surrounded by other atoms, leading to considerable fine structure in angular distributions at all polar angles. In contrast, when the adatoms are located *in* or *above* the surface plane, as in the case of Cu on Si(111) and O on Cu(001), strong anisotropies are observed only at low polar angles. However, as was shown for $CoSi_2$/Si(111), determination of the surface structure for systems where intermixing occurs is a rather difficult task requiring the calculation of several trial geometries, and is the subject of an entirely separate investigation. The problem is made even more difficult by the fact that the structure of the GaAs(001) surface is not yet known. In light of these difficulties, and since our interests in the present investigation are broader than just the structure of the first ML, we will not pursue the subject any further at this time.

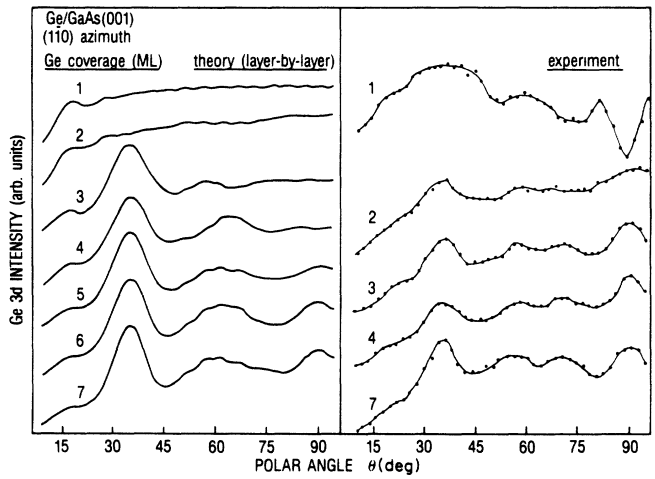

FIG. 6. Same as Fig. 4, only in the $(1\bar{1}0)$ azimuth.

Upon the addition of a second ML, we see the appearance of peaks at 35° in both (110) and $(1\bar{1}0)$, as well as a peak at 45° in (010). Comparison with the theoretical PAD's shows that these features betray the formation of at least a partial *third* layer by this coverage. There is even evidence of partial *fifth*-layer formation, as judged by the appearance of weak peaks at 90° in (110) and $(1\bar{1}0)$. By 3 ML, peaks at 90° are clearly present in all three azimuths, indicating that partial fifth-layer formation has definitely occurred. For coverages above 3 ML, the PAD's do not change significantly. The peak structure becomes better defined, but no new peaks appear. Together with the steady attenuation of the substrate signal (Fig. 3), the continuous improvement in the LEED pattern, and good agreement with theory, this result establishes that overlayer formation is not occurring by means of phase-segregated island formation. However, the appearance of certain features in the experimental PAD's at coverages that are lower than expected on the basis of theory strongly suggests that there is a statistical distribution of layer thickness across the surface of the order of 2–4 Å during the early stages of epitaxy, which probably remains at higher coverages.

Finally we note that neither the LEED pattern nor the XPD results for a 7-ML Ge epifilm grown and investigated one layer at a time as described above differ in any appreciable way from those for a 7-ML film grown all at once at 320 °C. In either case, we obtain PAD's like those shown at the bottom of the right-hand panels of Fig. 4–6 and a $p(2\times2)$ LEED pattern. We also obtain these results when we grow a 7-ML film on a surface that has been sputtered and annealed to give the $c(8\times2)$ reconstruction. In all cases, the excellent agreement between XPD theory and experiment at higher coverages indicates that the structural quality of the epifilm itself is quite good, although as the above analysis shows, atomic steps do exist on the surface.

The general appearance of RHEED patterns has led previous investigators to conclude that Ge layers on GaAs (001) prepared by first growing a buffer layer of GaAs are atomically smooth, whereas subsequent growth of GaAs on Ge leaves the surface with atomic-scale roughness (of the order of 3–5 Å).[1,2] However, oscillations in the specular RHEED beam intensity during growth of both Ge on GaAs(001) and GaAs on Ge(001) indicate that at no point is the surface as atomically

smooth as the starting substrate.[3] In both cases, well-defined oscillations are observed with periods corresponding to the time required for the completion of a monolayer. However, the absolute intensity drops significantly during the growth of the first layer and does not recover its original value, even after the sources are shut off. This observation is expected if there is a statistical distribution of layer thickness across the surface, as our XPD data indicate. Therefore, even when a given monolayer equivalent of atoms has impinged upon the surface and condensed, there exists some density of atomic steps. A reduction in the specular-beam and diffracted-beam intensities relative to the starting surface then results due to partial destructive interference. This relationship between surface morphology and intensity oscillations in diffracted RHEED beams has been previously noted[32] and modeled using a Markov description.[33]

B. Band-bending behavior at the interface

The use of high-resolution XPS to measure band bending and valence-band offsets at semiconductor interfaces has been firmly established.[11,25,34,35] First, it is necessary to accurately measure the energy difference between shallow core levels and the valence-band maximum for clean semiconductor surfaces. It is then possible to follow the motion of the bands by obtaining measurements of core-level binding energies after interface formation and subtracting the valence-band to core-level energy difference for the clean surface. In essence, this practice amounts to referencing the valence-band maximum to a shallow core level. Since substrate core levels are relatively easy to accurately measure after interface formation, this approach allows one to follow the valence-band maximum relative to the Fermi level in a reliable way. Furthermore, more than one core level can be used when a compound semiconductor substrate is being investigated, thereby allowing separate determinations of the valence-band energy. We have used this approach to monitor the band-bending behavior of Ge epilayers on semi-insulating (si) GaAs(001). As a check of instrument accuracy and stability, we measured the Au $4f_{7/2}$ binding energy for a clean Au reference surface directly before and immediately after all measurements on the Ge/GaAs system and found the value to be 84.00 ± 0.02 eV.[36]

In Fig. 7 we show a broad XPS scan for the clean si GaAs(001) surface covering the valence bands and the Ga and As 3*d* core-level peaks. This spectrum, one of several obtained with different substrates prepared by the two means outlined in Sec. II, was obtained with a 600-μm x-ray beam diameter and a pass energy of 50 eV. In order to minimize the effect of surface-state emission and affect some measure of Brillouin-zone averaging, the sample was oriented for normal emission with a full angle of acceptance of 30°. To determine the energy of the valence-band maximum relative to the Fermi level, we have extrapolated the leading edge of valence-band emission to the energy axis. Although this procedure is less satisfying than fitting the experimental data to a Gaussian-broadened, theoretical valence-band density of states, we have found that it leads to the same result within an uncertainty of ±0.02 eV.[37] The core levels were fitted using

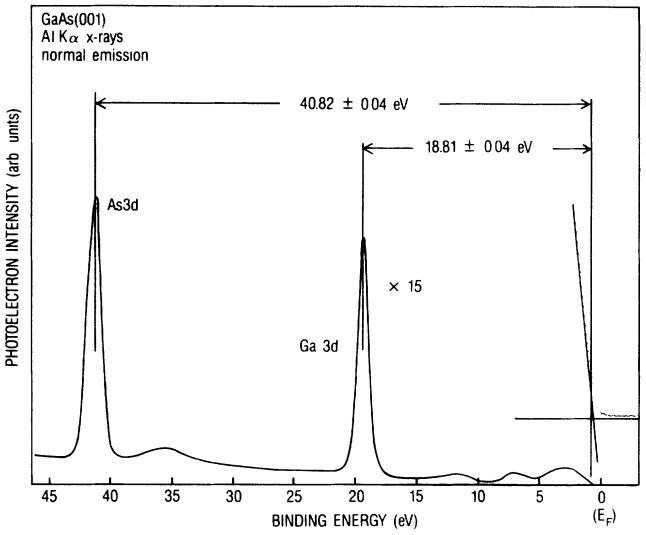

FIG. 7. As 3*d*, Ga 3*d*, and valence-band x-ray photoelectron spectrum from clean, semi-insulating GaAs(001) at normal photoelectron emission. The energy difference between the two-core levels and the valence-band maximum are shown with their respective experimental uncertainties, and are used to determine the Schottky-barrier height (see text). The zero in energy is taken to be the Fermi level.

a combination Gaussian (90%) and Lorentzian (10%) function. The As 3*d* spectrum was resolved into a spin-orbit doublet using a splitting of 0.71 eV and the statistical branching ratio of 0.67. No attempt was made to resolve the Ga 3*d* doublet. In the case of the As 3*d* spectrum, the centroid position was determined from a weighted average of the binding energies of the two spin-orbit components.

The Ga 3*d* and As 3*d* binding energies we measure in performing a broad scan which includes the valence bands are within 0.02 eV of the values we get by obtaining a much narrower scan over each core level individually, further substantiating the accuracy and stability of the spectrometer. The resulting values for the valence-band maximum to core-level energy difference are 18.81 ± 0.04 eV and 40.82 ± 0.04 eV for Ga 3*d* and As 3*d*, respectively. These numbers are within experimental error of the most recent numbers reported by Waldrop *et al.*,[35] although our values are consistently higher by a few hundredths of an eV. Using a value of 1.424 eV for the band gap of GaAs,[38] we can then express the SBH in terms of the Ga and As 3*d* core-level binding energies as

$$\Phi_b = \begin{cases} 20.23\pm0.04 - E_{\text{Ga }3d} \\ 42.24\pm0.04 - E_{\text{As }3d} \end{cases} . \quad (1)$$

Utilizing Eq. (1), we have measured the SBH of 12 different si GaAs(001) samples prepared as described in Sec. II. We have observed barrier heights ranging from 0.76 to 0.93 eV, with an average and standard deviation of 0.83 and 0.05 eV, respectively. The constancy of the Au $4f_{7/2}$ binding energy (84.00 ± 0.02 eV) during the course of these experiments demonstrates that the deviation in SBH from sample to sample represents true varia-

tions in the surface band bending, rather than a drift in the spectrometer electronics. This average SBH value for si GaAs(001) is intermediate between those reported for *n*-type GaAs(001), 0.71 eV,[11] and *p*-type GaAs(001), ~0.9.[39]

We show in Fig. 8 Ga and As 3*d* core-level spectra for clean GaAs(001) and the substrate with a 9-Å (6.4-ML) coverage of As-doped Ge which has been exposed to different heat treatments. Also shown are the SBH values as determined by Eq. (1). This particular sample exhibited clean-surface SBH values of 0.93 and 0.90 eV for Ga and As emission, respectively. The numbers in parentheses are the uncertainties in the last digit of each energy. Upon deposition of a thin overlayer of As-doped Ge, the SBH is observed to drop by ~0.4 eV. However, the SBH rises back to the clean-surface value of ~0.9 eV after three successive 10-min anneals at 225, 275, and 380 °C. Interestingly, the deposition of 9 Å of *undoped* Ge onto GaAs(001) (spectra not shown) does not significantly change the SBH relative to the clean surface (+0.05 eV, on average). Such films of undoped Ge have been found to be *p* type on several kinds of substrates.[40]

A more complete representation of the dependence of SBH and composition on annealing history for the sample discussed above is shown in Fig. 9. In the bottom panel we plot the As 3*d*– and Ga 3*d*–derived SBH values for the clean surface, the interface immediately after deposition, and the interface after annealing for 10 min at temperatures ranging from 175 to 380 °C. The Ga 3*d* to As 3*d* intensity ratio corrected for Scofield photoemission cross section[41] and the absolute Ge 3*d* intensities are plotted in the top panel. Upon codeposition of the Ge and As, the Ga to As ratio drops from the clean-surface value of 1.27 down to 1.04 as the SBH falls. Inasmuch as Ga 3*d* and As 3*d* electrons have very nearly identical escape

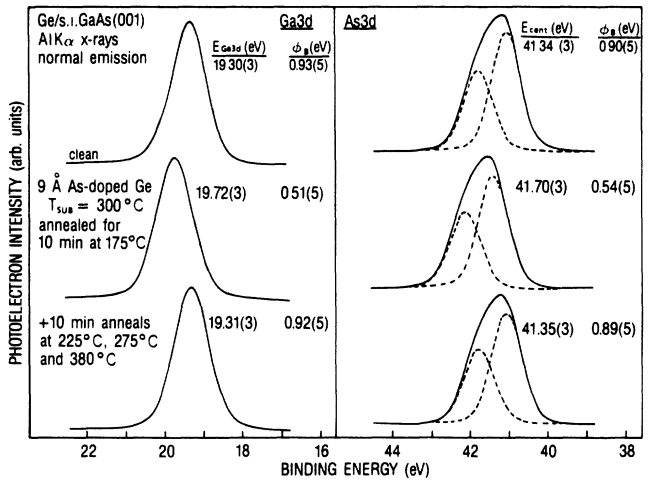

FIG. 8. Representative Ga and As 3*d* spectra for 9 Å of As-doped Ge on semi-insulating GaAs(001). The substrate temperature was 300 °C during growth. These data show the range of motion of the Schottky-barrier height as a result of different annealing treatments. The numbers in parentheses are the uncertainties in the last digit.

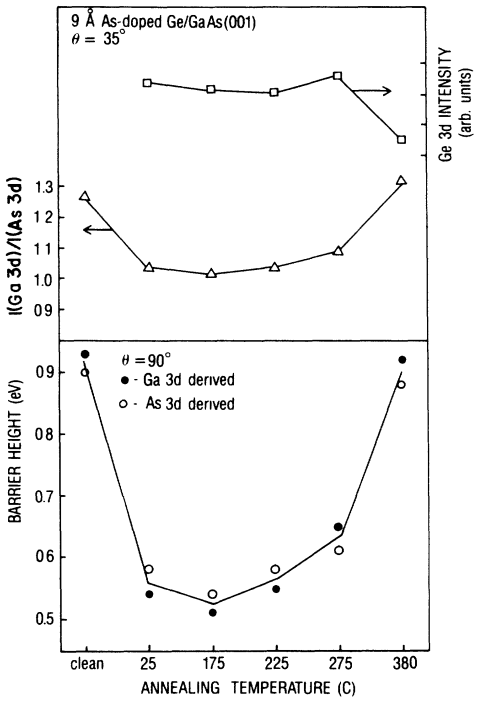

FIG. 9. XPS intensities (upper panel) and Schottky-barrier height (lower panel) plotted as a function of heat treatment for 9 Å of As-doped Ge on semi-insulating GaAs(001). The Ga 3*d* to As 3*d* ratio has been corrected for Scofield photoelectric cross section. The barrier height is clearly correlated with the dopant concentration in the Ge overlayer (see text).

depths, this result means that As has been incorporated into the Ge overlayer. The source of the As could either be the As boat in the MBE system or out-diffused As from the substrate. Evaporation of undoped Ge on GaAs(001) at a substrate temperature of 320 °C showed no evidence of As out-diffusion. Therefore, we conclude that we have coevaporated As and Ge with no significant disruption of the substrate. In this case, Ga and As 3*d* intensities from the substrate are attenuated by equal amounts, and the As incorporated into the Ge overlayer decreases the Ga to As ratio. Upon annealing at 175 °C the Ga to As ratio is reduced slightly more to 1.02 and the SBH also drops by another 0.04 eV. Anneals at temperatures above 175 °C cause a loss of As in the overlayer and a corresponding rise in the SBH. As the figure shows, the SBH is clearly correlated with the dopant (As) level in the overlayer. After annealing at 380 °C, the Ga to As ratio rises above the clean-surface value, presumably due to the total loss of As from the overlayer and perhaps some outdiffusion of Ga from the substrate. The SBH also rises back to the value for the clean surface and that for undoped Ge. Since it is known that Ge epilayers are degenerate *p* type when grown on GaAs at 325 °C,[11,42] it comes as no surprise that there is no difference between the SBH of undoped Ge on GaAs(001) and that for the Ga-doped Ge/GaAs which we believe results from annealing the interface to 380 °C. There is also a drop in the Ge signal after the final anneal, indicating

some loss of Ge from the near-surface region.

Comparison of the present work with that of Grant *et al.* for As- and P-doped Ge on *n*-type GaAs(001) shows that although the starting position of the Fermi level within the band gap differs by ~0.1 eV, the range of motion of the Fermi level is nearly the same, ~0.4 eV. This result further supports the conclusion that *n*-type Ge prevents pinning of the GaAs Fermi level and allows the Fermi level to move closer to the conduction band in response to the dopant concentration in the Ge.[11,12] However, this Fermi-level motion is not accompanied by any change in the valence-band discontinuity. Changes in the Ge 3*d* binding energy for the experiments summarized in Fig. 9 track with those observed in the Ga 3*d* and As 3*d* binding energies to within 0.1 eV. From these data, and valence-band maximum to core-level energy differences published by Waldrop *et al.*,[35] we determine that the valence-band offset is 0.60±0.05 eV for Ge/si-GaAs(001) independent of the Ge doping. This value agrees well with the analogous number as measured by XPS for *n*-type GaAs(001), 0.56 eV.[43] Although 0.56–0.60 eV is higher by ~0.1 eV than that reported by Chiaradia *et al.* for undoped Ge grown on several of the different reconstructions of sputtered and annealed GaAs(001),[12] the conclusion we draw is the same—that establishment of the Fermi level within the band gap is independent of the formation of the band-edge discontinuity.

IV. CONCLUSIONS

We have combined MBE growth capability with *in situ* structural and electronic characterization to investigate the nature of epitaxial growth and band-bending behavior of *n*- and *p*-type Ge epilayers on si GaAs(001). We find that the initial stages of epitaxy lead to a statistical distribution of layer thickness of the order of 2–4 Å for growth at 320 °C, a result which is consistent with RHEED beam-intensity oscillations but not recognized by previous investigators. Despite a nonzero step density on the surface, the structural quality of the resulting epilayers is excellent, as judged by good agreement between experimental and theoretical x-ray photoelectron diffraction results in which perfect epitaxy is assumed for the calculations. As doping of the Ge epilayers leads to a ~0.4 eV reduction in the Schottky-barrier height of the clean surface and the undoped-Ge/si-GaAs(001) interface. Furthermore, the barrier height scales directly with dopant level in the overlayer. Comparison of the present results with previous work on *n*-type GaAs(001) demonstrates that although the barrier height of the surface of semi-insulating material is 0.1 eV higher than that for *n*-type crystals, the magnitude of the barrier-height lowering is the same when *n*-type Ge overlayers are grown on either surface. Furthermore, the valence-band offset of the Ge/GaAs(001) interface appears to be independent of doping level in either the substrate or the overlayer, which further supports the conclusion that different mechanisms are responsible for the establishment of the Fermi level within the band gap and formation of the band discontinuity.

ACKNOWLEDGMENTS

The authors are pleased to acknowledge helpful and stimulating discussions with Dr. R. W. Grant, Dr. J. R. Waldrop, and Dr. K. Kuhn.

[1]C.-A. Chang, J. Appl. Phys. **53**, 1253 (1982).
[2]C.-A. Chang and T.-S. Kuan, J. Vac. Sci. Technol. B **1**, 315 (1983).
[3]J. H. Neave, P. K. Larsen, B. A. Joyce, J. P. Powers, and J. F. van der Veen, J. Vac. Sci. Technol. B **1**, 668 (1983).
[4]T.-S. Kuan and C. A. Chang, J. Appl. Phys. **54**, 4408 (1983).
[5]C.-A. Chang and W.-K. Chu, Appl. Phys. Lett. **42**, 463 (1983).
[6]R. A. Stall, C. E. C. Wood, K. Board, N. Dandekar, L. F. Eastman, and J. Devlin, J. Appl. Phys. **52**, 4062 (1981).
[7]J. M. Ballingall, C. E. C. Wood, and L. F. Eastman, J. Vac. Sci. Technol. B **1**, 675 (1983).
[8]J. M. Ballingall, R. A. Stall, C. E. C. Wood, and L. F. Eastman, J. Appl. Phys. **52**, 4098 (1981).
[9]O. Y. Borkovskaya, N. L. Dmitruk, R. V. Konakova, N. N. Solatenko, and Y. A. Tkhorik, Phys. Status Solidi A **59**, 395 (1980).
[10]D. Gammon, R. Merlin, W. T. Beard, and C. E. C. Wood, Superlatt. Microstruct. **1**, 161 (1985).
[11]R. W. Grant and J. R. Waldrop, J. Vac. Sci. Technol. B **5**, 1015 (1987).
[12]P. Chiaradia, A. D. Katnani, H. W. Sang, Jr., and R. S. Bauer, Phys. Rev. Lett. **52**, 1246 (1984).
[13]J. Nassies and J. Contout, J. Appl. Phys. **58**, 806 (1985).
[14]C. S. Fadley and S. A. L. Bergstrom, Phys. Lett. **35A**, 375 (1971).
[15]S. A. Chambers, I. M. Vitromirov, S. B. Anderson, H.-W. Chen, T. J. Wagener, and J. H. Weaver, Superlatt. Microstruct. **3**, 563 (1987).
[16]C. S. Fadley, in *Progress in Surface Science*, edited by S. G. Davison (Pergamon, New York, 1984), pp. 275–387.
[17]S. A. Chambers, S. B. Anderson, and J. H. Weaver, Phys. Rev. B **32**, 581 (1985).
[18]E. L. Bullock and C. S. Fadley, Phys. Rev. B **31**, 1212 (1985).
[19]M. Owari, M. Kudo, Y. Nihei, and H. Kamada, J. Electron Spectrosc. Relat. Phenom. **34**, 215 (1984).
[20]M. Owari, M. Kudo, Y. Nihei, and H. Kamada, Jpn. J. Appl. Phys. **24**, L394 (1985).
[21]P. Alnot, J. Olivier, F. Wyczisk, and C. S. Fadley, J. Electron Spectrosc. Relat. Phenom. **43**, 263 (1987).
[22]S. Y. Tong, H. C. Poon, and D. R. Snider, Phys. Rev. B **32**, 2096 (1985).
[23]M. Sagurton, E. L. Bullock, R. Saiki, A. Kaduwela, C. R. Brundle, C. S. Fadley, and J. J. Rehr, Phys. Rev. B **33**, 2207 (1986).
[24]M. P. Seah and W. A. Dench, Surf. Interface Anal. **1**, 2 (1979).
[25]E. A. Kraut, R. W. Grant, J. R. Waldrop, and S. P. Kowalczyk, Phys. Rev. B **28**, 1965 (1983).
[26]S. A. Chambers, S. B. Anderson, H.-W. Chen, and J. H.

Weaver, Phys. Rev. B **35**, 2592 (1987).
[27]S. A. Chambers, T. J. Wagener, and J. H. Weaver, Phys. Rev. B **36**, 8992 (1987).
[28]D. A. Steigerwald and W. F. Egelhoff, Jr., Surf. Sci. (to be published).
[29]S. A. Chambers, S. B. Anderson, H.-W. Chen, and J. H. Weaver, Phys. Rev. B **34**, 913 (1986).
[30]R. Saiki, a. Kaduwela, J. Osterwalder, M. Sagurton, and C. S. Fadley, J. Vac. Sci. Technol. A **5**, 932 (1987).
[31]S. Kono, S. M. Goldberg, N. F. T. Hall, and C. S. Fadley, Phys. Rev. B **22**, 6085 (1980).
[32]P. I. Cohen, P. R. Pukite, J. M. Van Hove, and C. S. Lent, J. Vac. Sci. Technol A **4**, 1251 (1986).
[33]C. S. Lent and P. I. Cohen, Surf. Sci. **139**, 121 (1984).
[34]E. A. Kraut, R. W. Grant, J. R. Waldrop, and S. P. Kowalczyk, Rev. Lett. **44**, 1620 (1980).
[35]J. W. Waldrop, R. W. Grant, and E. A. Kraut, J. Vac. Sci. Technol. B **5**, 1209 (1987), and references therein.
[36]F. R. McFeely, S. P. Kowalczyk, L. Ley, R. A. Pollak, and D. A. Shirley, Phys. Rev. B **7**, 5228 (1973).
[37]We performed this extrapolation in Figs. 6 and 8 of Ref. 25, where experimental spectra for GaAs(110) and Ge(110) were fitted to Gaussian-broadened theoretical valence-band densities of states and found that the extrapolation yields very nearly the same zero in energy as does the fit. We then employed this approach to find the valence-band maximum in our data, as shown in Fig. 7.
[38]S. M. Sze, *Physics of Electron Devices* (Wiley, New York, 1981), p. 850.
[39]R. W. Grant, J. R. Waldrop, S. P. Kowalczyk, and E. A. Kraut, J. Vac. Sci. Technol. **19**, 477 (1981).
[40]J. E. Davey, Appl. Phys. Lett. **8**, 164 (1966).
[41]J. Scofield, J. Electron Spectrosc. Relat. Phenom. **8**, 129 (1976).
[42]S. P. Kowalczyk, R. W. Grant, J. R. Waldrop, and E. A. Kraut, J. Vac. Sci. Technol. B **1**, 684 (1983).
[43]J. R. Waldrop (private communication).